Rapid Microwave Synthesis and Structural Phase Diagram of $Ln_xY_{1-x}MnO_3$

Fred P. Marlton[a], Darren J. Goossens[a], Reyner White[a], and Wayne D. Hutchison[b]

[a] Research School of Chemistry, The Australia National University, Canberra, ACT 0200, Australia

[b] School of Physical, Environmental and Mathematical Sciences, University of New South Wales, Canberra 2600, Australia

Reprint requests to Dr. Darren Goossens. E-mail: goossens@rsc.anu.edu.au

Z. Naturforsch. **2014**, *69b*, 761 – 766 / DOI: 10.5560/ZNB.2014-4065
Received March 18, 2014

$YMnO_3$ is one of the primary examples of a multiferroic ceramic. We present a novel solid-state microwave sintering method for making high-purity ceramic samples of $YMnO_3$ and related compounds in a few hours. This leads to determination of the structural phase diagram for the formation of single-phase, hexagonal samples when doping lanthanides into $YMnO_3$. It is found that the solid-state microwave synthesis allows manufacture of high-quality samples in hours rather than days. The resulting phase diagram accords well with results from the literature, and from calculations based on the Goldschmidt tolerance factor for the stability of perovskite structures, suggesting that the transformation from hexagonal to perovskite with doping is driven essentially by ion sizes. Some results concerning the microwave synthesis of Ba*Ln*InO_4 compounds, where *Ln* is a lanthanide, are noted. Microwave sintering of $BaNdInO_4$ yields single-phase samples where conventional sintering does not.

Key words: Yttrium Manganate, Phase Diagram, Ba*Ln*InO_4, $YMnO_3$, Microwave Synthesis

Introduction

Multiferroic materials have been of significant interest in recent years due to their ability to exhibit both ferroelectric and magnetic order. Compounds of the type *Ln*MnO_3 (*Ln* = Y and La – Lu) display this multiferroic behaviour [1]. Studies have been conducted on these materials to better understand the relationship between the ferroelectric and magnetic orderings [2 – 9].

The *Ln*MnO_3 materials are obtained in one of two different structures. For large *Ln* ions (*Ln* = La – Tb) the orthorhombic perovskite structure is observed, whereas for the small *Ln* ions (*Ln* = Y, Ho – Lu) the hexagonal structure is observed [2, 10].

Conventional solid-state synthesis of these materials generally relies on temperatures around 1400 °C and sintering times of the order of 85 hours in resistively heated furnaces [11, 12]. It has been reported that using microwave furnaces for solid-state synthesis can substantially reduce the time required for sintering [13, 14]. A study of BCZT ($Ba_{0.95}Ca_{0.05}Zr_{0.25}Ti_{0.75}O_3$) revealed significant improvement in relaxor behaviour as well as reductions in energy and time required for synthesis through the use of microwave sintering. The faster heating and cooling rates involved in microwave synthesis caused a decrease in grain size [15]. Compared to results from conventional sintering, microwave sintered alumina-titania ceramics show higher density, finer and more homogeneous microstructure, higher strength, higher hardness and higher fracture toughness [16].

However, direct sintering of ceramic powders using microwaves is an underused approach in solid-state synthesis, partly because the products of the process tend to lack systematic behaviour, and as a result synthetic procedures are often developed on an *ad hoc* basis. However, due to the speed and efficiency of the microwave approach, finding ways of using it to synthesise important and interesting, and potentially industrial, materials is of value. This is emphasised by the increasing availability of moderately-priced off-the-shelf microwave furnaces. Given that researchers can now purchase identical furnaces, a synthesis undertaken in one lab is transferable to other laboratories,

something more difficult when furnaces are bespoke and unique.

Experimental Section

Microwave synthesis

Polycrystalline 1 g samples of $Y_{1-x}Ln_xMnO_3$ were synthesised by solid-state reaction using a microwave furnace. In a microwave process, heat is generated within the material by the absorption of microwaves so that the thermal gradient and the resulting flow of heat is the reverse of that found in conventional heating [15, 17].

Stoichiometric amounts of Y_2O_3, MnO_2 and Ln_2O_3 (or Pr_6O_{11}) were thoroughly mixed by grinding in a mortar with a pestle, and then pressed into 13 mm pellets. The samples were sintered in a Synotherm HAMiLab-ADS 1.5 kW microwave sintering system using the temperatures and durations outlined in Table 1. Total oven time was 5 h 40 min, of which 2 hr 30 min was spent ramping, an order of magnitude less than typically found in the literature [11, 12]. Between the different sintering temperatures the samples were allowed to cool and then re-ground and pelleted to ensure thorough mixing.

Lanthanides used included La, Pr, Nd, Sm, Eu, Gd, Tb, Dy, Ho, Er, and Yb as well as In, while x varied from 0 (pure $YMnO_3$) to 0.5.

X-Ray diffraction

Powder XRD data were collected using a PANalytical Empyrean diffractometer with a sample spinner, using CuK_α radiation. Data were collected over an angular range of $10^\circ \leq 2\theta \leq 100^\circ$ with a step size of 0.01313° and a scan speed of $0.051491^\circ\,s^{-1}$. Data from XRD scans were then refined by the Rietveld technique using Rietica [18] to determine phase purity, lattice parameters and other key structural parameters. Fig. 1 shows the refinement for a sample of $YMnO_3$. The specimen is single phase, and the structure is hexagonal.

Table 1. Sample preparation conditions using the microwave furnace.

Sinter Number	Temp. (°C)	Time to ramp (min, from r. t.)	Time at temp. (min)
1	800	30	30
2	1100	50	60
3	1400	70	100

Discussion

The parameters of the fit shown in Fig. 1 are summed up in Table 2. Oxygen atomic displacement parameters (ADPs) are often not well constrained by X-ray data when much heavier atoms are present, and so these values were taken from a survey of the literature of similar compounds. This is not an issue here, as this study is predominantly concerned with the success or otherwise of the synthesis route and mapping out the phase diagram.

The phases that formed for the samples synthesised are summarised in Fig. 2. The phases and the solubility limits accord well with results using more conven-

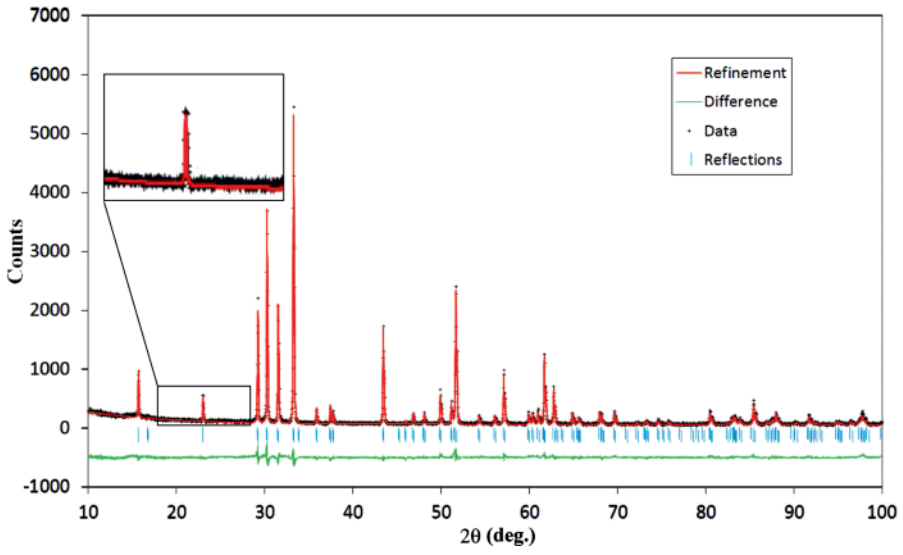

Fig. 1. Diffraction pattern of $YMnO_3$, synthesised using microwave sintering of ceramic precursors. The inset shows a close up view of the region 18 to 28°, showing the absence of impurity peaks.

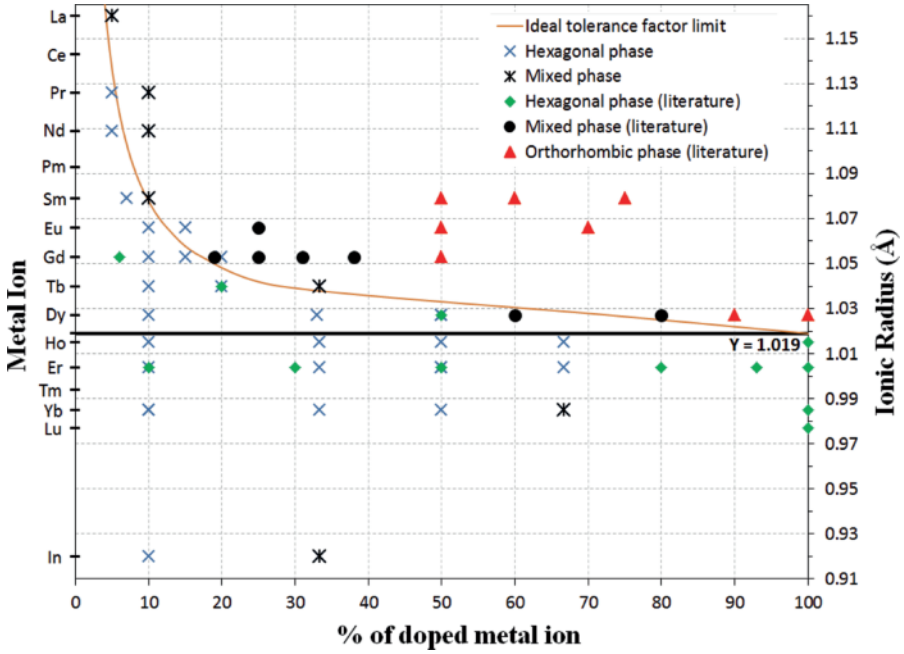

Fig. 2. Phase diagram for the $Y_{1-x}Ln_xMnO_3$ system. The vertical axis gives the dopant metal ion, *Ln*, with ionic size in Å listed on the right. The horizontal axis represents the percentage of doping, *x*. The simple crosses (×) and diamonds (♦) represent hexagonal samples from the microwave syntheses and from the literature, respectively. The barred crosses (✕) and filled circles (•) give mixed-phase samples from the microwave syntheses and from the literature, respectively, while the triangles (▲) indicate orthorhombic phases found in the literature. The solid curved line (–) on the plot represents the theoretical limit based upon the tolerance factor, Eq. 1. The horizontal black line at 1.019 Å gives the radius of yttrium. Data for Sm-doped samples from [23], Eu from [24], Gd from [25], Tb from [12], Dy from [2], Er from [26], Yb and Lu from [27].

Table 2. Refined structural parameters for $YMnO_3$, synthesised using microwave sintering of ceramic precursors. $a = 6.1418(3)$ Å, $c = 11.4020(6)$ Å, space group is $P6_3cm$. Underlines indicate refined parameters, parentheses indicate estimated uncertainties. Note that oxygen B_{iso} could not be well-determined from these data. Y1 and Y2 B_{iso} were constrained to be equal.

Atom	*x*	*y*	*z*	B_{iso} (Å^2)
O1	0.316(1)	0	0.167(1)	1.97
O2	0.631(1)	0	0.346(1)	1.97
O3	0	0	0.483(1)	1.97
O4	1/3	2/3	0.022(1)	1.97
Mn	0.3151(5)	0	0	0.45(1)
Y1	0	0	0.2723(2)	0.99(1)
Y2	1/3	2/3	0.2326(2)	0.99(1)

tional approaches, suggesting that it is very much the intrinsic chemistry which is most strongly governing the formation of these phases

The Goldschmidt tolerance factor, *t*, is widely used to predict whether the ions will form a perovskite-like structure. If R_O is the radius of oxygen, R_B that for the B-site and R_A for the A-site cation [19], then

$$t = \frac{R_O + R_A}{\sqrt{2}\,(R_O + R_B)} \qquad (1)$$

and the perovskite structure is likely to be stable for $t > 0.8$. Setting $t = 0.8$ allows calculation of the limiting value of *x* for a given dopant ion, *Ln*. This gives rise to the curved orange line in Fig. 2. If the assumption is made that when the perovskite structure is untenable the hexagonal structure forms, this should give an approximation of the phase boundary, and this is seen to be the case. This suggests quite strongly that ionic size effects determine the stability of the hexagonal phase.

Structural trends

The relationship between the *a* parameter of the hexagonal structure and the average A-site radius is

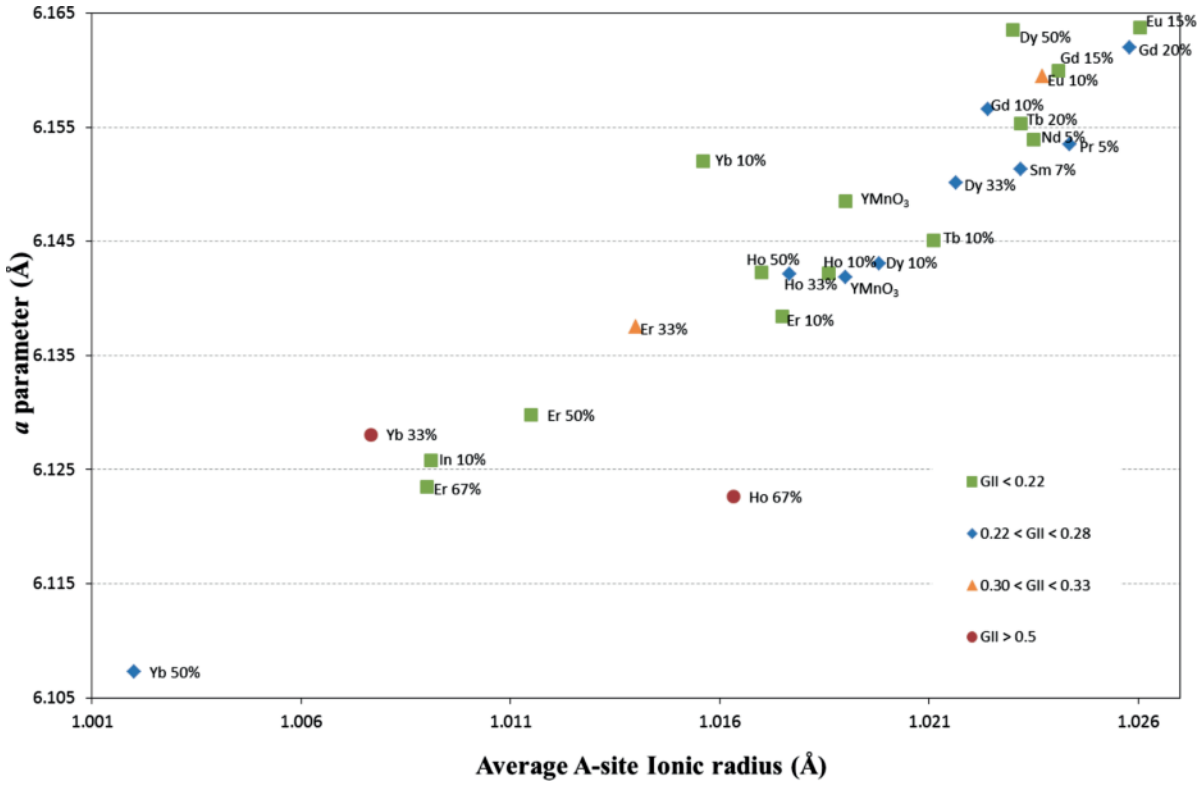

Fig. 3. The a ($= b$) lattice parameter of the hexagonal $Y_{1-x}Ln_xMnO_3$ system, plotted against average A-site radius. The trend is apparent. The colours of the markers encode the global instability index of the Rietveld-refined structures [28 – 30]; most are within acceptable limits. Two samples of $YMnO_3$ were produced and measured, and the spread in these two values gives an indication of uncertainty. No similar trend was apparent in c.

plotted in Fig. 3, and shows a strong trend. This is absent in the c parameter, as has been noted previously [20]. The reason for the anisotropic lattice expansion lies in the coordination of the A-site cations. In directions lying in the ab plane, the A-site cations and oxygen ions make a strong network of atoms, while along c there is one long A-site to oxygen distance ($\sim$ 3.3 Å) and one much shorter distance ($\sim$ 2.4 Å) (Fig. 4). The bond valence [21] of the longer bond is very small, approximately 0.04 valence units, while for the shorter it is still relatively small, but an order of magnitude larger. Hence, the contribution to the bonding of the A-site cations from the oxygen anions along c is very small, allowing larger atoms to be accommodated without causing expansion along c. The dense network of much shorter bonds in the other directions results in strong correlation between the a length and the average A-site cation size.

Synthesis of $BaLnInO_4$

It is known that $BaLaInO_4$ can be synthesised using a sol-gel approach [22]; it is of interest to explore (1) whether a solid-state synthesis route can be found and (2) what other lanthanides can be substituted for La. A comparison of conventional and microwave sintering of these potential ionic conductors has been undertaken. The general formula is $AA'BO_4$, (where A is Ba, A' is a lanthanide and B is In). The starting oxide powders (or carbonate in the case of Ba) were first milled under acetone before being pressed into 13 mm pellets. These pellets were then placed into a conventional furnace at 950 °C for several hours to decompose the carbonate, before they were removed, crushed and pressed again to ensure a homogeneous composition. The new pellets were then placed (a) in a conventional furnace with a ramp rate of 10 °C min^{-1} to reach 1390 °C and left to react for 24 h and (b) in a mi-

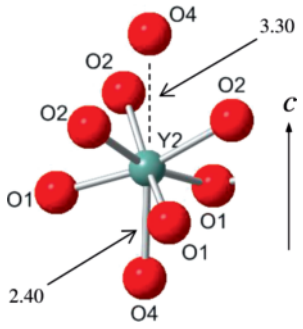

Fig. 4. The bonding environment of the Y2 atom, showing the long bonds along c (3.3 Å and 2.4 Å) and the more densely packed oxygen atoms in the other directions.

crowave furnace at a temperature of 1300 °C, at a ramp rate of 18.5 °C min^{-1} for a sintering time of 3 h. In all cases a bed of the initial starting powder was laid down inside the alumina crucible to act as a barrier between it and the sample pellet. The overall reaction scheme is as follows:

$$2\ BaCO_3 + In_2O_3 + Ln_2O_3 \Rightarrow$$
$$2\ BaLnInO_4 + 2\ CO_2$$

$BaLaInO_4$ is a Ruddlesden-Popper phase with $n = 1$ [31, 32], and in the solid-state syntheses attempted here, the $n = 2$ phase, $BaLa_2In_2O_7$, was found to be formed preferentially, both in conventional and microwave sintering.

By reducing the Ba stoichiometry to $Ba_{0.96}NdInO_4$, to minimise production of some Ba-rich impurity phases, microwave sintering yielded what is thought to be a sample of "$BaNdInO_4$"; however while a unit cell ($a = 17.654(1)$, $b = 6.025(2)$, $c = 4.123(2)$ Å, $\beta = 90.283(3)°$) and likely space group ($P2_1$) have been identified, the material appears to be a previously unreported structure type, and a full structural solution is currently work-in-progress. Samples of $BaLnInO_4$ with Ln = Ho, Er, and Dy were made and showed a common, new phase; but a second phase was also present. Attempts to produce Gd and Sm samples proved unsuccessful.

Conclusions

It has been demonstrated that samples of the type $Y_{1-x}Ln_xMnO_3$ can be synthesised using rapid microwave techniques. The total sintering time for these samples is slightly greater than 5 h. Hence, use of the microwave furnace can result in an order of magnitude reduction in sintering time for solid-state synthesis. Against this is the lack of systematic behaviour shown by microwave syntheses, and this is the core of why the microwave technique is difficult: a material's response to microwaves varies with temperature and microwave frequency, and when new phases are dynamically forming during the heating it is very difficult to predict how the absorption of energy will vary with time and temperature. If the experimenter is prepared to invest some time in trials, the rapidity of the microwave sintering means that systems to be synthesised can be screened quickly, and, if promising, conditions can easily be optimised. When a synthesis takes hours instead of days or weeks, it is not so important if the results are unpredictable. This speed also aids in mapping out the phase diagram.

In this case, the composition range of $Y_{1-x}Ln_xMnO_3$ for which the hexagonal phase is formed – with samples sintered in air and not under pressure – has been mapped out, particularly when Ln is larger in radius than Y. The phase boundary follows the perovskite tolerance factor limit quite closely, and agrees with results of conventional syntheses from the literature, suggesting that the microwave sintering is in this case not resulting in substantial structural differences compared to conventional processes, although this study does not explore microstructure, and grain size may well be affected.

Acknowledgement

D. J. G. thanks the Australian Research Council for financial support. He thanks Dr. Aidan Heerdegen for LaTeX help and Dr. Lasse Norén for experimental assistance. R. W. thanks Prof. R. L. Withers.

[1] B. B. Van Aken, T. T. M. Palstra, A. Filippetti, N. A. Spaldin, *Nat. Mater.* **2004**, *3*, 164.
[2] H. S. Nair, C. M. N. Kumar, H. L. Bhat, S. Elizabeth, T. Brückel, *Phys. Rev. B* **2011**, *83*, 104424.
[3] T. Katsufuji, M. Masaki, A. Machida, M. Moritomo, K. Kato, E. Nishibori, M. Takata, M. Sakata, K. Ohoyama, K. Kitazawa, H. Takagi, *Phys. Rev. B* **2002**, *66*, 134434.

[4] G. A. Smolenskii, I. E. Chupis, *Sov. Phys. Usp.* **1982**, *25*, 475.
[5] S. C. Abrahams, *Acta Crystallogr. B* **2009**, *65*, 450.
[6] A. S. Gibbs, K. S. Knight, P. Lightfoot, *Phys. Rev. B* **2011**, *83*, 094111.
[7] S. Lee, A. Pirogov, M. Kang, K.-H. Jang, M. Yonemura, T. Kamiyama, S.-W. Cheong, F. Gozzo, N. Shin, H. Kimura, Y. Noda, J.-G. Park, *Nature* **2008**, *451*, 805.
[8] A. Muñoz, J. A. Alonso, M. J. Martínez-Lope, M. T. Casáis, J. L. Martínez, M. T. Fernández-Díaz, *Phys. Rev. B* **2000**, *62*, 9498.
[9] D. G. Tomuta, S. Ramakrishnan, G. J. Nieuwenhuys, J. A. Mydosh, *J. Phys.: Condens. Matter* **2001**, *13*, 4543.
[10] J. S. Helton, D. K. Singh, H. S. Nair, S. Elizabeth, *Phys. Rev. B* **2011**, *84*, 064434.
[11] S. D. Kaushik, S. Rayaprol, *AIP Conference Proceedings* **2012**, *1447*, 1299.
[12] H. N. Li, J. W. Huang, L. X. Xiao, L. P. Peng, Y. Y. Wu, G. H. Du, Z. W. Ouyang, B. R. Chen, Z. C. Xia, *J. Appl. Phys.* **2012**, *111*, 083913.
[13] A. Agostino, P. Benzi, M. Castiglioni, N. Rizzi, P. Volpe, *Supercond. Sci. Techn.* **2004**, *17*, 685.
[14] H. Liu, S. Bi, G. Wen, X. Teng, P. Gao, Z. Ni, Y. Zhu, F. Zhang, *J. Alloys Compd.* **2012**, *543*, 99.
[15] S. Mahajan, O. Thakur, D. Bhattacharya, K. Sreenivas, *Mater Chem. Phys.* **2008**, *112*, 858.
[16] H. Bian, Y. Yang, Y. Wang, W. Tian, H. Jiang, Z. Hu, W. Yu, *J. Alloys Compd.* **2012**, *525*, 63.
[17] W. Sutton, *Ceram. Bull.* **1989**, *68*, 376.
[18] B. Hunter, *International Union of Crystallography Commission on Powder Diffraction Newsletter* **1998**, 20.
[19] R. D. Shannon, *Acta Crystallogr.* **1976**, *A32*, 751.
[20] M. C. Sekhar, S. Lee, G. Choi, C. Lee, J.-G. Park, *Phys. Rev. B* **2005**, *72*, 014402.
[21] N. E. Brese, M. O'Keeffe, *Acta Crystallogr.* **1991**, *B47*, 192.
[22] Y. A. Titov, N. Belyavina, V. Markiv, M. Slobodyanik, Y. Krayevska, *Dopov. Nats. Akad. Nauk Ukr., Mat. Pryr. Tekh. Nauky* **2009**, *10*, 160.
[23] D. O'Flynn, C. V. Tomy, M. R. Lees, G. Balakrishnan, *J. Phys.: Conf. Ser.* **2010**, *200*, 012149.
[24] J. Hemberger, F. Schrettle, A. Pimenov, P. Lunkenheimer, V. Y. Ivanov, A. A. Mukhin, A. M. Balbashov, A. Loidl, *Phys. Rev. B* **2007**, *75*, 035118.
[25] J.-W. G. Bos, B. B. van Aken, T. T. M. Palstra, *Chem. Mater.* **2001**, *13*, 4804.
[26] O. P. Vajk, J. Gunasekera, Y. Wang, T. Heitmann, *J. Appl. Phys.* **2011**, *109*, 07D910.
[27] T. Katsufuji, S. Mori, M. Masaki, Y. Moritomo, N. Yamamoto, H. Takagi, *Phys. Rev. B* **2001**, *64*, 104419.
[28] I. Etxebarria, J. M. Perez-Mato, A. García, P. Blaha, K. Schwarz, J. Rodriguez-Carvajal, *Phys. Rev. B* **2005**, *72*, 174108.
[29] A. Santoro, I. N. Sora, Q. Huang, *J. Solid State Chem.* **2000**, *151*, 245.
[30] A. Salinas-Sanchez, J. Garcia-Muñoz, J. Rodriguez-Carvajal, R. Saez-Puche, J. Martinez, *J. Solid State Chem.* **1992**, *100*, 201.
[31] S. N. Ruddlesden, P. Popper, *Acta. Crystallogr.* **1957**, *10*, 538.
[32] S. N. Ruddlesden, P. Popper, *Acta. Crystallogr.* **1958**, *11*, 54.